Dual-chirp Arbitrary Microwave Waveform Generation by Using a Dual Parallel Mach-Zehnder Modulator Feeding with RF Chirp Signal

**Sanjeev Kumar Raghuwanshi[*], Ritesh Kumar,
Akash Srivastava, and Nimish Kumar Srivastava**

Abstract—In this paper, dual-chirped arbitrary microwave waveform has been generated through photonics, incorporated with single dual parallel mach-zehnder modulator (DPMZM) inbuilt mach zehnder interferometer (MZI) structure. We have taken two cases of chirping, i.e., linear and nonlinear chirps. A case of linear chirping has been explored previously. However, to the best of the authors' knowledge effect of nonlinear chirping in this paper is evaluated for the first time. Other photonics approaches are also available, such as spectra shaping and wavelength to time mapping. But due to fixed spectral response of spectral shaper, center frequency of linear chirp generated waveform is fixed. To get large center frequency again we have to use large number of spectral shapers which will increase the system complexity. DPMZM avoids such difficulties. These MZMs are biased at the minimum transmission point to get carrier suppressed modulation. Product modulator (PM) is cascaded to the lower arm of DPMZM. Here by using DPMZM we get two advantages. First we have two complimentarily chirped microwave waveforms and second up conversion of the frequency of microwave carrier. A dual-chirped microwave waveform with centre frequency 6 GHz with bandwidth 200 MHz and 2 GHz is generated. The paper gives specific details about various performance parameters such as input signal frequency and power, output signal parameters viz output frequency, chirp rate, chirp bandwidth, time bandwidth product (TBW), etc. The overall model and its performance parameters are computed through MATLAB simulation.

1. INTRODUCTION

Range resolution of Radar can be improved by compressing a pulse, since range error is directly proportional to pulse width. Such a compressed pulse is linearly chirped microwave waveform. Among different types of ambiguity function, i.e., Knife edge (Ridge), Bed of spikes, and thumbtack, linear frequency modulated waveforms or linear chirped microwave waveform has ridge type ambiguity function, which reduces range Doppler resolution since such a waveform has large range Doppler coupling. But, a dual-chirped microwave waveform has much smaller Doppler coupling which gives high range Doppler resolution [1–4]. A dual-chirped microwave waveform contains two signal components. One is up chirped and the other down chirped waveform. Chirped microwave waveform is generated using modern photonics technique, which gives higher centre frequency and larger bandwidth than that generated by other means, i.e., conventional circuits may be analogue or digital circuits [5, 6]. This paper basically deals with dual-chirped arbitrary microwave waveform generation by using single dual parallel mach zehnder modulator (DPMZM) inbuilt mach zehnder interferometer (MZI) structure. We have taken two cases of chirping, i.e., linear and nonlinear chirps with clear mathematical derivation behind the results.

* Corresponding author: Sanjeev Kumar Raghuwanshi (sanjeevrus@yahoo.com).
The authors are with the Electronics Engineering Department, Indian School of Mines Dhanbad, Jharkhand 826004, India.

2. CASE OF LINEAR CHIRPING: PRINCIPAL AND THEORY

A schematic diagram of a dual-chirp microwave generation system having a single DPMZM is shown in Figure 1. An optical signal with frequency ω_0 generated by laser diode (LD) is first passed through polarization controller (PC), and then it is given to DPMZM. DPMZM consists of two arms, upper and lower arms. There is a PM incorporated with the lower arm of DPMZM. Outputs of sub-MZMs are combined at the output of DPMZM and passed to photo detector (PD). Output current of PD is proportional to the square of its input optical intensity. At the output of PD, high frequency terms are eliminated due to photo-detector band limiting nature. Finally, the signal is passed to a high pass filter (HPF) where lower order frequency terms are eliminated, and we get the desired waveform at the output of HPF. Input optical signal to the dual parallel mach-zehnder modulator (DPMZM) is $E_0 e^{j\omega_0 t}$ where, E_0 is the amplitude of optical field and ω_0 the input frequency [7–21].
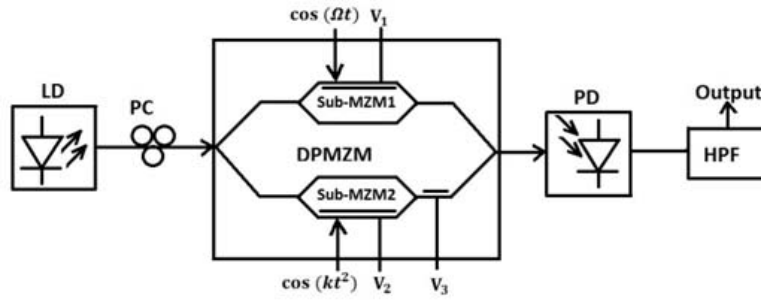
Figure 1. Dual-Chirp microwave generation system.

Output of the upper arm, i.e., sub MZM-1, is,

$$E_{out1} = \frac{E_0}{2} e^{j\omega_0 t} e^{j\Delta\emptyset_1 t} \tag{1}$$

Output of the lower arm, i.e., sub MZM-2, is,

$$E_{out2} = \frac{E_0}{2} e^{j\omega_0 t} e^{j\Delta\emptyset_2 t} \tag{2}$$

$\Delta\emptyset_1$ and $\Delta\emptyset_2$ are the phase changes due to sub MZM-1 and 2, respectively.

$$\Delta\emptyset_1 = \frac{\pi V_1 \cos(\Omega t)}{V_{\pi_1}} = \beta_1 \cos(\Omega t) \quad \text{and,} \quad \Delta\emptyset_2 = \frac{\pi V_2 \cos(kt^2)}{V_{\pi_2}} = \beta_2 \cos(kt^2)$$

where $\frac{\pi V_2}{V_{\pi_2}} = \beta_2$, V_1 and V_2 are the amplitudes of the signals applied at sub MZM-1 and 2, respectively. Both sub-MZMs are biased at the minimum transmission point. Here double sideband carrier suppressed modulation has been used. Microwave carrier signal is $\cos(\Omega t)$ with Ω as the carrier frequency applied at MZM-1, and $\cos(kt^2)$ is the baseband signal with k as the chirp rate is applied at MZM-2. Here, this chirping is linear since rate of change of frequency with respect to time is constant. In the lower arm product modulator (PM) is cascaded to sub-MZM-2. Let $\emptyset_3$ be the phase introduced by product modulator. The optical output signal at the output of DPMZM is given by,

$$E(t) = \frac{E_0}{2} e^{j\omega_0 t} \left(e^{j\beta_1 \cos(\Omega t)} + e^{j\beta_2 \cos(kt^2)} e^{j\emptyset_3} \right) \tag{3}$$

Using Jacobi-Anger expansion and simplifying above expression by taking double sidebands and suppressed carrier by setting $\frac{E_0}{2} = 1$,

$$E(t) = j \left[J_1(\beta_1) e^{j(\omega_0 - \Omega)t} + J_1(\beta_1) e^{j(\omega_0 + \Omega)t} + J_1(\beta_2) e^{j(\omega_0 - kt^2 + \emptyset_3)} + J_1(\beta_2) e^{j(\omega_0 + kt^2 + \emptyset_3)} \right] \tag{4}$$

Output of photo detector is proportional to the optical intensity, as it is the square law device.

$$i_o(t) \propto |E(t)|^2$$

$$\therefore i_o(t) \propto \left| J_1\left(\beta_1\right)\left(2\cos\left(\Omega t\right)\right) + J_1\left(\beta_2\right)e^{j\left(\emptyset_3\right)}2\cos\left(kt^2\right) \right|^2 \tag{5}$$

Only taking the AC term at the input of PD, due to band limited nature of photo diode, neglecting high frequency term containing $\cos\left(2\Omega t\right)$, finally at the output of high pass filter, low frequency term will be eliminated.

$$i_o(t)_{HPF} \propto 4J_1\left(\beta_1\right)J_1\left(\beta_2\right)\cos\emptyset_3\left[\cos\left(\Omega t - kt^2\right) + \cos\left(\Omega t + kt^2\right)\right] \tag{6}$$

Here, Ω denotes the centre frequency of the dual-chirp microwave waveform, and k decides the chirp rate and bandwidth of dual-chirp microwave waveform.

2.1. Properties of Ambiguity Function

It is the function of time delay and Doppler frequency, which shows the distortion of reflected signal due to matched filter. More Doppler shift gives rise to smaller peak of resulting waveform, and hence more difficult to detect the signal. Time delay between the transmitting signal and echo signal can be measured from distance, or range to the target. Frequency shift is the measure of relative velocity, or relative velocity can also be measured from the rate of change of range. Radar accuracy is defined by,

a. Geometrical representation between signal noise and parameter to be measured.
b. Inverse probability.
c. Suitable gating function proceeded by matched filter
d. Estimate of variance using likelihood function.

Ambiguity function is given by,

$$|\chi\left(\tau, f_d\right)|^2 = \left| \int_{-\infty}^{\infty} i(t)i^*(t-\tau)e^{j2\pi f_d t}dt \right|^2 \tag{7}$$

In ambiguity diagram, $\tau = positive\ value$ indicates the target beyond the reference delay. $f_d = positive\ value$ indicates incoming target.

Ambiguity function is used to define the transmitted waveform through target resolution, measurement accuracy, ambiguity and response to clutter. Properties of ambiguity function.

Maximum value of

$$|\chi(\tau, f_d)|^2 = |\chi(0.0)|^2 = (2E)^2 \tag{8}$$

where, $E = Energy\ of\ the\ signal$

$$|\chi(-\tau, -f_d)|^2 = |\chi\left(\tau, f_d\right)|^2 \tag{9}$$

$$|\chi(\tau, 0)|^2 = |u(t)u^*\left(t - \tau\right)|^2 \tag{10}$$

$$|\chi(0, f_d)|^2 = \left| \int u^2(t)e^{j2\pi f_d t}dt \right|^2 \tag{11}$$

$$\iint |\chi(\tau, f_d)|^2\, d\tau df_d = (2E)^2 \tag{12}$$

Equation (8) indicates that the maximum value of ambiguity function occurs at origin, and its value is $(2E)^2$. Here Equation (9) indicates its symmetric behaviour. Equation (10) indicates the behaviour of ambiguity function on time-delay axis, whereas Equation (11) shows its behaviour on Doppler frequency axis. Along time delay axis $\chi(\tau, f_d)$ is autocorrelation of $u(t)$. Also along frequency axis it is spectrum of $u^2(t)$. Hence Equation (12) indicates that the total volume under ambiguity function is constant, i.e., $(2E)^2$.

2.2. Ideal Ambiguity Function

Ideal ambiguity function has a single spike with infinitesimal thickness at the origin. The single spike shows no ambiguity, and infinitesimal thickness permits to find frequency and echo delay time simultaneously with very high accuracy. It also permits the resolution of two targets even they are at any minimum closest distance on ambiguity diagram. Shortening pulse width gives rise to range accuracy but at the expense of Doppler velocity accuracy, i.e.,

$$\text{Range error} \propto \tau, \quad \text{and} \quad \text{Doppler error} \propto \frac{1}{\tau}$$

$|\chi(0,0)|^2$ is the indication of detection capabilities of Radar. For the detection of target, ambiguity diagram is rarely used since in the plot of ambiguity diagram, $|\chi(0,0)|^2 = 1$, i.e., Normalised. Accuracy of range and velocity can be measured by a particular waveform which depends upon the width of the spike centered at $|\chi(0,0)|^2$ along the time and frequency axes. Resolution is related with the width of the centre spike, but to resolve two closely spaced targets the central spike must be isolated. For the proper detection energy of waveform should be sufficiently large, and receiver should match filter. Waveform shape is only important for the design of matched filter.

2.3. Derivation of Ambiguity Function

The single chirp microwave waveform which can be obtained from Equation (6) as follows

$$i_s(t) = \frac{1}{\sqrt{T}} rect\left(\frac{t}{T}\right) e^{j(\Omega t \pm k t^2)} \quad -\frac{T}{2} \leq t \leq \frac{T}{2} \tag{13}$$

In above expression, positive sign is for up-chirp and negative sign for down chirp. Also, we have taken normalized function so that it follows some rules from statistics. Normalized means that probability of finding particle somewhere will be 100%.

$$\frac{1}{\sqrt{T}} rect\left(\frac{t}{T}\right) = \frac{1}{\sqrt{T}} \quad for, |t| \leq \frac{T}{2}$$
$$= 0 \quad for, |t| > \frac{T}{2} \tag{14}$$

From Equation (7), ambiguity function for single chirp signal is given by,

$$|\chi(\tau, \Omega_d)|^2 = \left| \int_{-\infty}^{\infty} i_s(t) i_s^*(t - \tau) e^{j\Omega_d t} dt \right|^2; \quad \tau \geq 0 \quad \text{and} \quad \Omega_d = 2\pi f_d$$
$$i_s(t - \tau) = \frac{1}{\sqrt{T}} rect\left(\frac{t - \tau}{T}\right) e^{j\left(\Omega(t-\tau) \pm k(t-\tau)^2\right)}; \quad -\frac{T}{2} \leq t - \tau \leq \frac{T}{2} \tag{15}$$
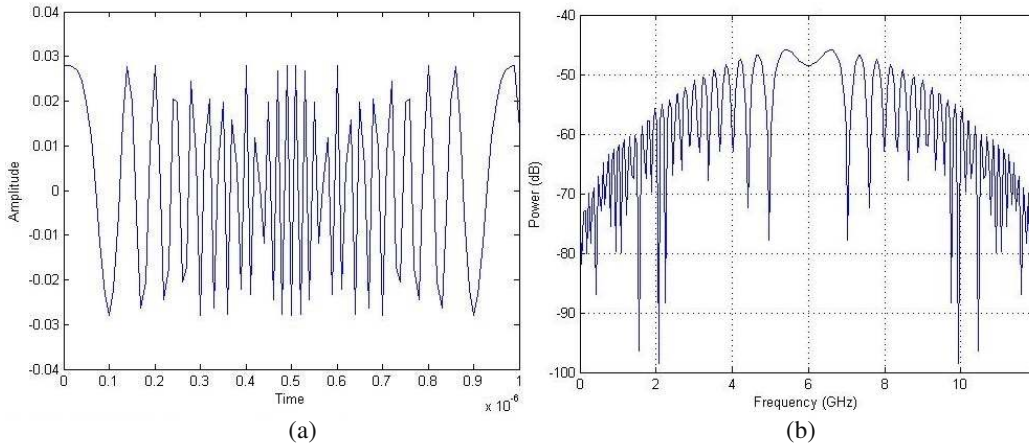$$= 0 \quad ; otherwise$$

Now,

$$i_s^*(t - \tau) = \frac{1}{\sqrt{T}} \left[rect\left(\frac{t - \tau}{T}\right) \right]^* e^{-j\left(\Omega(t-\tau) \pm k(t-\tau)^2\right)} \quad ; -\frac{T}{2} \leq t - \tau \leq \frac{T}{2} \tag{16}$$
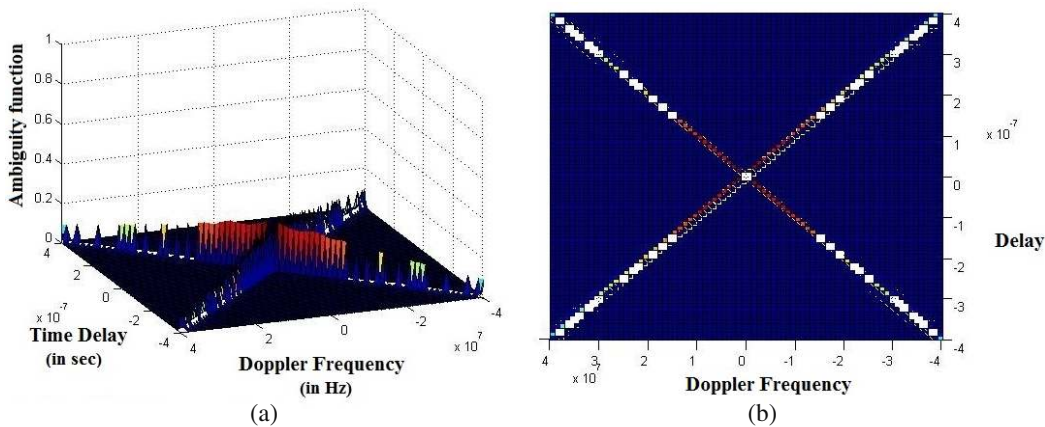
$$|\chi_s(\tau, \Omega_d)|^2 = \left[\left(1 - \frac{\tau}{T}\right) \frac{\sin\left(\frac{T}{2}(2k\tau \pm \Omega_d)\left(1 - \frac{\tau}{T}\right)\right)}{\left(\frac{T}{2}\right)(2k\tau \pm \Omega_d)\left(1 - \frac{\tau}{T}\right)} \right]^2 \tag{17}$$

Dual-chirp microwave waveform is given by,

$$i_d(t) = \frac{1}{\sqrt{2}} \frac{1}{\sqrt{T}} Rect\left(\frac{t}{T}\right) \left[e^{j\left(\Omega t + k t^2\right)} + e^{j\left(\Omega t - k t^2\right)} \right]; \quad -\frac{T}{2} \leq t \leq \frac{T}{2} \tag{18}$$

Figure 2. (a) Dual-chirped microwave waveform (amplitude versus time) and (b) power spectrum of dual-chirped signal.
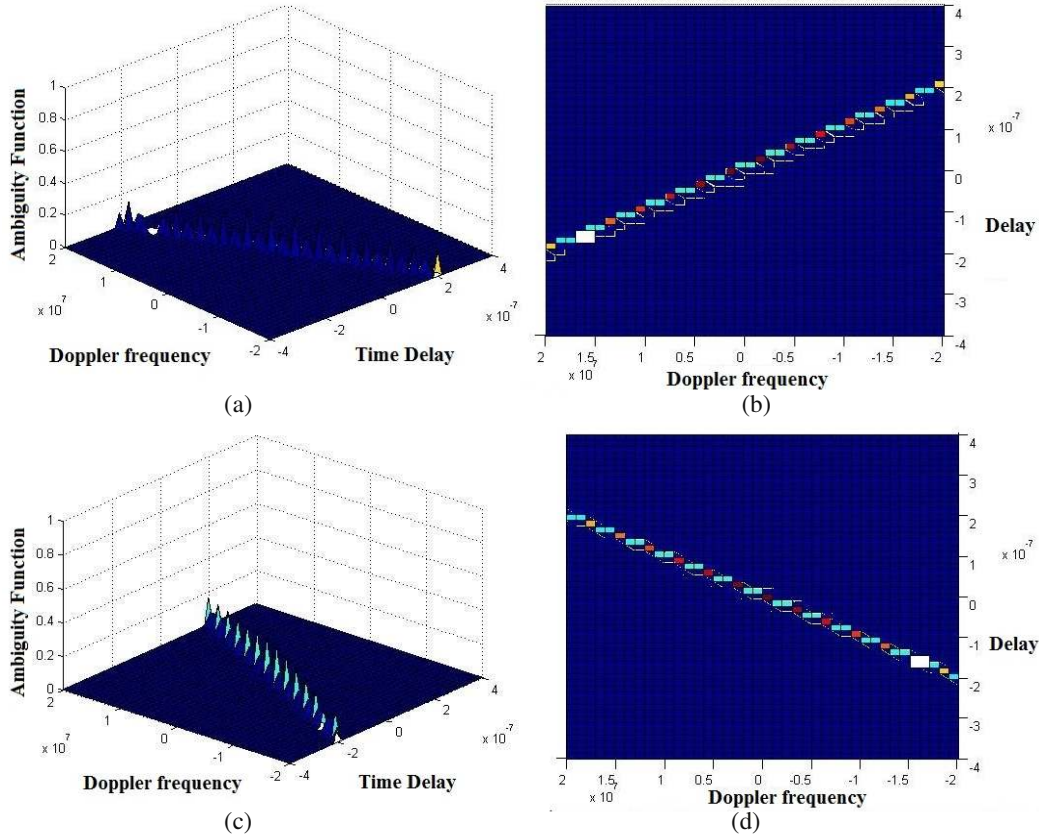

Figure 3. (a) Ambiguity functions versus time and frequency. (b) Ambiguity function versus time and frequency (top view).

Plot of the above equation is shown in Figures 2(a) and 2(b). Figure 2(a) shows the plot of amplitude versus frequency, and Figure 2(b) shows the plot of power versus frequency. Here the signal power is normalized. Same as Equation (17), ambiguity function for dual-chirp microwave waveform is given by,

$$|\chi_d\left(\tau,\Omega_d\right)|^2 = \frac{1}{4}\left[\left(1-\frac{\tau}{T}\right)\frac{\sin\left(\frac{T}{2}\left(2k\tau+\Omega_d\right)\left(1-\frac{\tau}{T}\right)\right)}{\left(\frac{T}{2}\right)\left(2k\tau+\Omega_d\right)\left(1-\frac{\tau}{T}\right)} + \left(1-\frac{\tau}{T}\right)\frac{\sin\left(\frac{T}{2}\left(2k\tau-\Omega_d\right)\left(1-\frac{\tau}{T}\right)\right)}{\left(\frac{T}{2}\right)\left(2k\tau-\Omega_d\right)\left(1-\frac{\tau}{T}\right)}\right]^2 \quad (19)$$

Plot of ambiguity function of Equation (19) is shown in Figure 3(a). Its top view is given in Figure 3(b). Figures 4(a) and (b) show the single down chirped ambiguity function and its top view, respectively. Similarly, Figures 4(c) and (d) show the single up chirped ambiguity function and its top view, respectively. Bandwidth of dual-chirped waveform can be tuned by tuning the chirp rate of baseband single chirp waveform. Previous plots have been simulated for the chirp rate of $\pi \times 10^{14}\,\mathrm{s}^{-2}$, centre frequency 6 GHz and time duration of pulse 1 μs. By changing chirp rate to $10^{15}\,\mathrm{s}^{-2}$, dual-chirped microwave waveform is shown in Figure 5(a). Figure 5(b) is the plot between its power and frequency. Figure 6 is the plot of ambiguity function for new chirp rate.

Power spectrum of dual-chirped microwave waveform having linear chirping shown by Figure 2(b) has its peak power located at the center frequency of 6 GHz in the frequency span 0–10 GHz. It is also
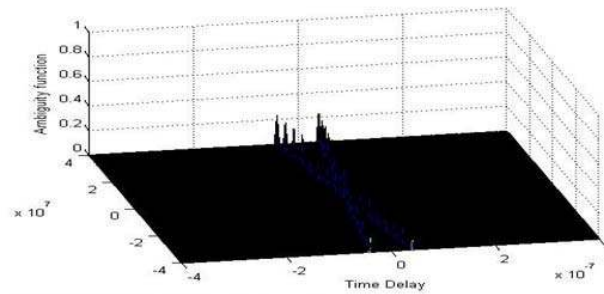
Figure 4. (a) Ambiguity function versus time and frequency (single down chirped). (b) Ambiguity function versus time and frequency (single down chirped) top view. (c) Ambiguity function versus time and frequency (single up chirped). (d) Ambiguity function versus time and frequency (single up chirped) top view.
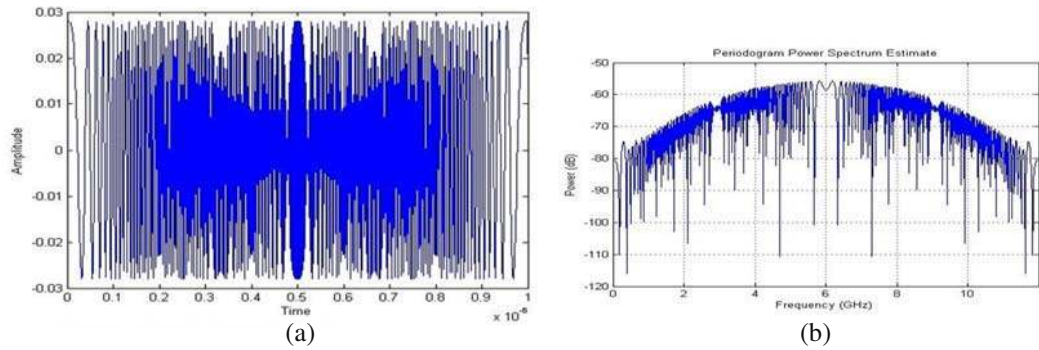
Figure 5. (a) Dual-chirped waveform (amplitude (volt) versus time (s)). (b) Power spectrum of Dual-chirped waveform.

apparent from the above figure that side lobes are located on both sides of the main lobe while power decrease when moving away from the center frequency.

Ambiguity function shown in Figure 3(a) is symmetric about the origin. Multiple spikes occur in ambiguity diagram. Strength of the spikes decreases when moving away from the origin of diagram, i.e., ambiguity function has spikes of greatest amplitude near the origin. Ambiguity function for the single up and down chirping can also be seen. Above diagram shows the same and its contour map.

**Figure 6.** Ambiguity function versus time and frequency.

Figure 5(a) represents the dual-chirped microwave waveform for the increased value of chirp rate applied to MZI. As can be seen by Figures 2(a) and 5(a), with increasing the applied chirp rate to the MZI the microwave signal generated is highly chirped for the same time duration of pulse signal.

Power spectrum is almost the same even increasing the chirp rate with the same center frequency of 6 GHz. Here bandwidth has been reduced. In both cases, bandwidth is in the range of hundreds of MHz. In Figures 2(a) and (b), dual-chirp waveform and its spectrum is seen in frequency span 0 to 12 GHz respectively. It is clear that dual microwave chirp signal has been generated which has time duration of 1 µs and bandwidth 2 GHz centred at frequency of 6 GHz. Ambiguity function shown for up and down chirping is knife-edge shaped. Dual-chirp ambiguity function is symmetric about the origin, and the spike strength decreases with moving away from the origin. This phenomenon does not occur for single up and down chirp signal, which shows that dual-chirp microwave waveform will increase the Doppler resolution in a Radar system.

Further increasing the chirp rate to $\pi \times 10^{15}\,\text{s}^{-2}$, main to side lobe ratio is improved in ambiguity diagram for dual-chirp waveform.

3. SPECIFIC CASE OF NONLINEAR CHIRPING

Schematic diagram for the generation of dual-chirp microwave signal is shown Figure 7. This figure is the same as Figure 1 except the chirping used here is nonlinear. In this section, the expression for dual-chirp signal and its ambiguity function has been derived with suitable assumption, same as the case of linear chirping. All plots have been simulated again in MATLAB.
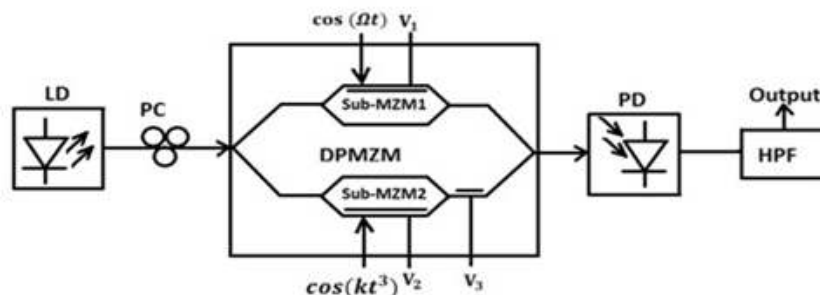
Figure 7. Dual-chirp microwave generation system (nonlinear chirping).

3.1. Developed Theory and Principal

In Figure 7, both sub-MZMs are biased at minimum transmission point so that carrier suppressed modulation will occur. V_1 and V_2 bias voltages are given at MZM1 and MZM2, respectively. Also $\cos(\Omega t)$ is the microwave carrier signal given to sub-MZM1. Here $\cos(kt^3)$ is the single chirp baseband signal with chirp rate k given to sub MZM2. To the best of our knowledge, the nonlinear chirping has

not been discussed previously. A product modulator is incorporated here in the lower arm of DPMZM. Input optical signal to the DPMZM (Dual parallel mach-zehnder modulator) is $E_0 e^{j\omega_0 t}$, where E_0 is the amplitude of optical field and ω_0 the input frequency. On the basis of mathematics used for Subsection 2.3, single nonlinear chirp microwave waveform is given by,

$$i_s(t) = \frac{1}{\sqrt{T}} rect\left(\frac{t}{T}\right) e^{j\left(\Omega t \pm kt^3\right)}; \quad -\frac{T}{2} \le t \le \frac{T}{2} \tag{20}$$

Dual-chirp microwave waveform is given by,

$$i_d(t) = \frac{1}{\sqrt{2}} \frac{1}{\sqrt{T}} rect\left(\frac{t}{T}\right) \left[e^{j\left(\Omega t + kt^3\right)} + e^{j\left(\Omega t - kt^3\right)}\right] \tag{21}$$

3.2. Ambiguity Function for Nonlinear Chirping with Comparison with Linear Chirping

In this section, we derive an accurate expression for the ambiguity function of nonlinear chirping case. From Equation (20),

$$i_s(t - \tau) = \frac{1}{\sqrt{T}} rect\left(\frac{t - \tau}{T}\right) e^{j\left(\Omega(t-\tau) \pm k(t-\tau)^3\right)} \tag{22}$$

$$i_s^*(t - \tau) = \frac{1}{\sqrt{T}} rect\left(\frac{t - \tau}{T}\right) e^{-j\left(\Omega(t-\tau) \pm k(t-\tau)^3\right)}; \quad -\frac{T}{2} \le t - \tau \le \frac{T}{2} \tag{23}$$

$\pm$ denotes up and down chirp waveforms. Ambiguity function in order to find the range Doppler resolution is given by,

$$|\chi(\tau, \Omega_d)|^2 = \left|\int_{-\infty}^{\infty} i_s(t) i_s^*(t - \tau) e^{j\Omega_d t} dt\right|^2 \tag{24}$$

τ is the delay time and Ω_d the Doppler frequency.

$$\chi(\tau, \mathbf{f_d}) = \int_{-\infty}^{\infty} i_s(t) i_s^*(t - \tau) e^{j\Omega_d t} dt = \frac{1}{T} e^{j\left(\Omega\tau \pm k\tau^3\right)} \int_{-\frac{T}{2}+\tau}^{\frac{T}{2}} e^{-j\left(-\Omega_d t \pm 3k\tau^2 t\right)} e^{\pm j3kt^2\tau} dt \tag{25}$$

Let, $a = \mp j3k\tau$ and, $b = j(-\Omega_d \pm 3k\tau^2)$.
    Putting in Equation (25),

$$\chi = \frac{1}{T} e^{j\left(\Omega\tau \pm k\tau^3\right)} \int_{-\frac{T}{2}+\tau}^{\frac{T}{2}} e^{-at^2} e^{-bt} dt \tag{26}$$

Simplifying above integration,

$$\chi = \frac{1}{T} e^{j\left(\Omega\tau \pm k\tau^3\right)} \left[\frac{\sqrt{\pi} e^{\frac{b^2}{4a}} erf\left(\frac{2at + b}{2\sqrt{a}}\right)}{2\sqrt{a}}\right]_{-\frac{T}{2}+\tau}^{\frac{T}{2}}$$

$$= \frac{1}{T} \frac{e^{j\left(\Omega\tau \pm k??^3\right)} \sqrt{\pi} e^{\frac{b^2}{4a}}}{2\sqrt{a}} \left[erf\left(\frac{aT + b}{2\sqrt{a}}\right) - erf\left(\frac{2a\left(-\frac{T}{2} + \tau\right) + b}{2\sqrt{a}}\right)\right]$$

$$\text{or}, \chi = \frac{1}{T} \frac{e^{j\left(\Omega\tau \pm k\tau^3\right)} \sqrt{\pi} e^{\frac{b^2}{4a}}}{2\sqrt{a}} \left[erf\left(\frac{aT + b}{2\sqrt{a}}\right) - erf\left(\frac{-aT + 2a\tau + b}{2\sqrt{a}}\right)\right] \tag{27}$$

For up chirping,

$$a = -j3k\tau \quad \text{and}, \quad b = j(-\Omega_d + 3k\tau^2) \tag{28}$$

For down chirping,
$$a = j3k\tau \quad \text{and,} \quad b = j(-\Omega_d - 3k\tau^2) \tag{29}$$

From Equation (27), ambiguity function is given by,
$$|\chi|^2 = \frac{1}{T^2} \left| \frac{\sqrt{\pi} e^{\frac{b^2}{4a}}}{2\sqrt{a}} \left[\text{erf}\left(\frac{aT+b}{2\sqrt{a}} \right) - \text{erf}\left(\frac{-aT+2a\tau+b}{2\sqrt{a}} \right) \right] \right|^2 \tag{30}$$

For up chirp waveform, ambiguity function is given by,
$$|\chi|^2 = \frac{1}{T^2} \left| \frac{\sqrt{\pi} e^{\frac{\left(j\left(-\Omega_d + 3k\tau^2\right)\right)^2}{-j12k\tau}}}{2\sqrt{-j3k\tau}} \right.$$
$$\left. \left[\text{erf}\left(\frac{-j3k\tau T + j\left(-\Omega_d + 3k\tau^2\right)}{2\sqrt{-j3k\tau}} \right) - \text{erf}\left(\frac{j3k\tau T - j6k\tau^2 + j\left(-\Omega_d + 3k\tau^2\right)}{2\sqrt{-j3k\tau}} \right) \right] \right|^2 \tag{31}$$

Down chirp waveform ambiguity function is,
$$|\chi|^2 = \frac{1}{T^2} \left| \frac{\sqrt{\pi} e^{\frac{\left(j\left(-\Omega_d - 3k\tau^2\right)\right)^2}{j12k\tau}}}{2\sqrt{j3k\tau}} \right.$$
$$\left. \left[\text{erf}\left(\frac{j3k\tau T + j\left(-\Omega_d - 3k\tau^2\right)}{2\sqrt{j3k\tau}} \right) - \text{erf}\left(\frac{-j3k\tau T + j6k\tau^2 + j\left(-\Omega_d - 3k\tau^2\right)}{2\sqrt{j3k\tau}} \right) \right] \right|^2 \tag{32}$$

Combining Equations (31) and (32), ambiguity function for dual nonlinearly chirp signal is given by,
$$|\chi(\tau,\Omega_d)|^2 =$$
$$\frac{1}{T^2} \left| \frac{\sqrt{\pi} e^{\frac{\left(j\left(-\Omega_d + 3k\tau^2\right)\right)^2}{-j12k\tau}}}{2\sqrt{-j3k\tau}} \left[\text{erf}\left(\frac{-j3k\tau T + j\left(-\Omega_d + 3k\tau^2\right)}{2\sqrt{-j3k\tau}} \right) - \text{erf}\left(\frac{j3k\tau T - j6k\tau^2 + j\left(-\Omega_d + 3k\tau^2\right)}{2\sqrt{-j3k\tau}} \right) \right] \right|^2 +$$
$$\frac{1}{T^2} \left| \frac{\sqrt{\pi} e^{\frac{\left(j\left(-\Omega_d - 3k\tau^2\right)\right)^2}{j12k\tau}}}{2\sqrt{j3k\tau}} \left[\text{erf}\left(\frac{j3k\tau T + j\left(-\Omega_d - 3k\tau^2\right)}{2\sqrt{j3k\tau}} \right) - \text{erf}\left(\frac{-j3k\tau T + j6k\tau^2 + j\left(-\Omega_d - 3k\tau^2\right)}{2\sqrt{j3k\tau}} \right) \right] \right|^2 \tag{33}$$

Plot of Equation (21) is shown in Figure 8(a). Pulse duration is 1 ns, and computed chirp rate rate is $\pi \times 10^{14}\,\text{s}^{-3}$. With the same parameters as for earlier case of linear chirping, for this case its power spectrum is shown in Figure 8(b). Similar plots of ambiguity function given by Equation (31) for up chirping and Equation (32) for down chirp cases are shown in Figure 9 and Figure 10, respectively. Also plot of ambiguity function given by Equation (33) and its contour plot for the dual-chirp signal are shown in Figure 11 and Figure 12, respectively.

Figure 8(a) shows a dual-chirp microwave waveform generated in the case of nonlinear chirping given to the MZI. Here the generated waveform is periodic in nature. Power spectrum for the dual nonlinear chirp signal has been plotted in the frequency span from $-3\,\text{GHz}$ to $3\,\text{GHz}$. However, power spectrum shown by Figure 8(b) is different from the power spectrum for linear chirping case. Here peak power is detected around the centre frequency of $0.4\,\text{GHz}$. From Figures 9 and 10 it is apparent that the ambiguity functions for up chirp and down chirp signals are different from that of linear chirping case. In early case of linear chirping, it was knife-edge shaped unlike the present case of nonlinear chirping. Here, there are large number of spikes along the delay line and parallel to Doppler frequency axis. We can see from Figures 9 and 10 that spikes come under the consideration for zero time delay. However, ambiguity function shown in Figure 11 has spikes everywhere on the plane, all having significant strength. Hence
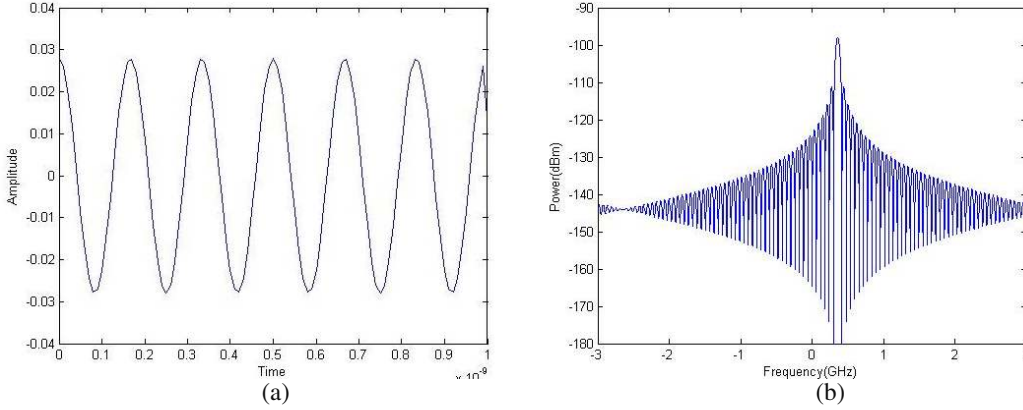
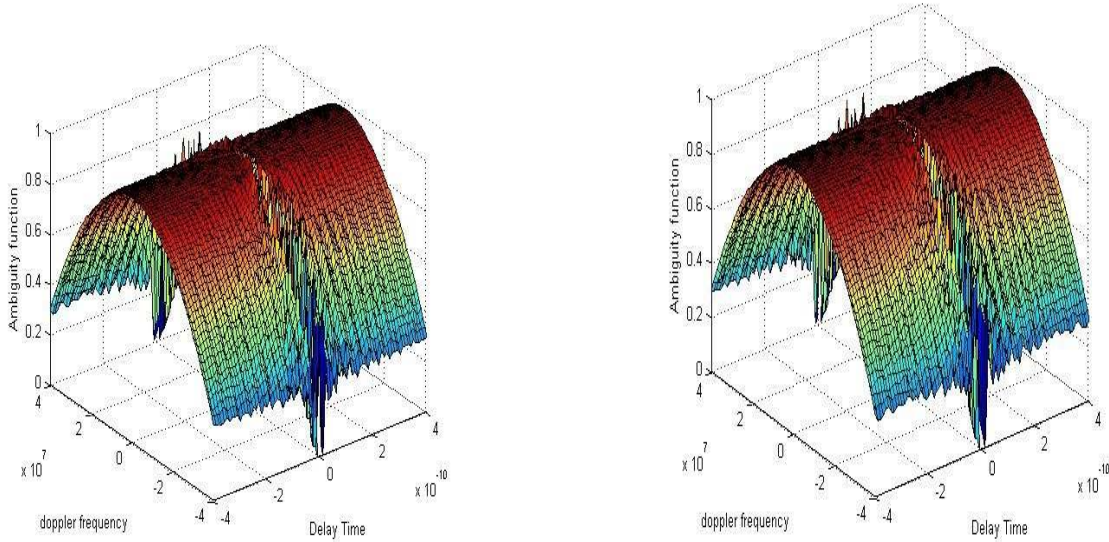**Figure 8.** (a) Dual-chirp microwave waveform. (b) Power spectrum of dual-chirp waveform.

**Figure 9.** Ambiguity function for up chirping.   **Figure 10.** Ambiguity function for down chirp.

this chirp rate does not provide desired result as clear as for ideal ambiguity function. This effect is also apparent from the contour plot given in Figure 12. There are continuous and dark lines crossing the time delay and Doppler frequency for zero values of delay and Doppler frequency. With keeping the same pulse duration to 1×10^{-6} s and increasing the chirp rate to $\pi \times 10^{19}$ s^{-3}, plot of dual-chirp microwave waveform and its power spectrum are shown in Figures 13(a) and (b). Ambiguity function for dual-chirp waveform and its contour plot are shown in the Figures 14(a) and (b), respectively. As we increase the chirp rate, change can be seen in the generated dual-chirp waveform by comparing Figures 8(a) and 13(a). The dual-chirp microwave waveform shown in Figure 13(a) has positive chirping. This waveform is quite different as shown by Figure 8(a).
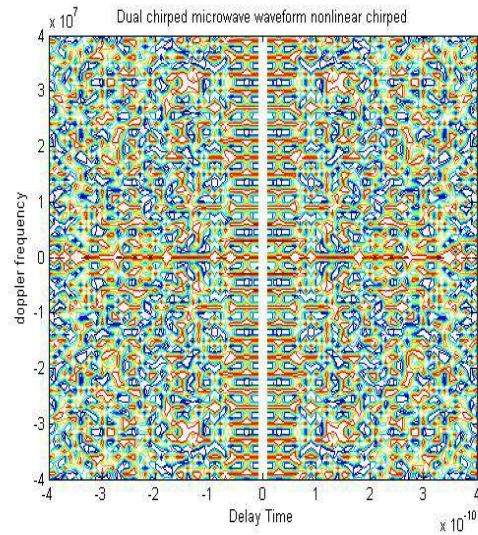
Dual-chirp microwave waveform shown in the earlier case has no clear chirping whereas the later one shown by Figure 13(a) is a chirp signal. Hence the increased value of chirp rate shows the chirping effect in generated microwave signal. This effect is more pronounced for the case of nonlinear chirping compared with linear chirping case.

Power spectrum shown by Figure 13(b) has also been changed, and it is apparent from the figure that the two generated waveforms have different bandwidths centered at the same frequency.

For the increased value of chirp rate, ambiguity function for dual nonlinearly chirped microwave waveform has also been changed. New ambiguity function is improved from the previous one, and it reduces ambiguity since there is no existence of spikes all over the plane of Doppler frequency and delay.
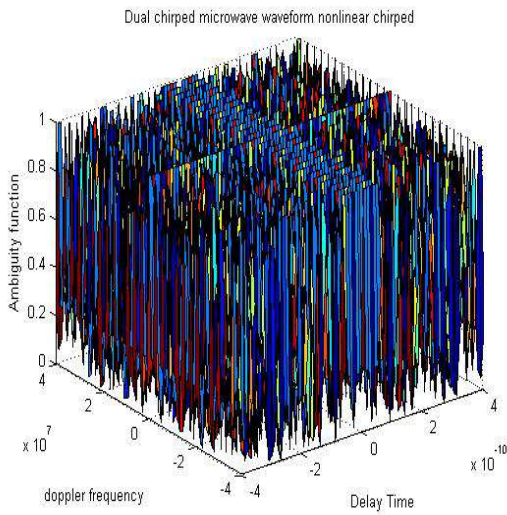
Figure 11. Ambiguity function for dual-chirp signal as a function of doppler frequency and doppler delay.


**Figure 12.** Contour plot of ambiguity function of dual-chirp signal.
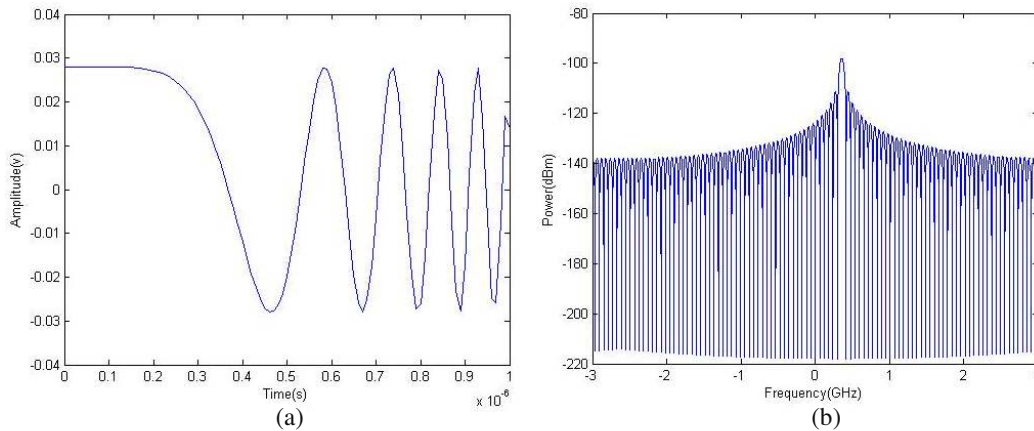
Figure 13. (a) Dual-chirp microwave waveform. (b) Power spectrum of dual-chirp signal.

Spikes occur only for nearly zero values of Doppler frequency. One more improvement here is that as delay time approaches the origin, the strength of ambiguity function increases and gets its maximum value near the origin. The MATLAB simulated contour map given by Figure 14(b) gives a clearer view. The presence of significant spikes only near the origin increases the Doppler resolution in Radar system. Again with increasing the chirp rate to $\pi \times 10^{20} \, \text{s}^{-3}$ by keeping the same pulse duration, all plots have been repeated as shown in Figures 15(a) to (d).

Chirping is more clearly shown by Figure 15(a). It is apparent from Figure 15(a) that dual-chirp microwave waveform is periodic in nature and shows both up and down chirping. Due to nonlinear chirping and time duration of pulse in microsecond range chirped signal comes into the figure for very high value of chirp rate. Power spectrum shown by Figure 15(b) gives the idea of bandwidth of a dual-chirp signal. Bandwidth of a dual-chirp signal in this case again has the same frequency range, i.e., in the order of tens of MHz. Ambiguity function for the chirp rate of $\pi \times 10^{20} \, \text{s}^{-3}$ is improved from the earlier cases as can be seen in Figure 15(c) and its counter map shown in Figure 15(d). It is apparent that ambiguity function is symmetric about the origin. Figure 15(d) reveals that the strength of spike is maximum at the origin, and it decreases significantly when moving away from the origin.
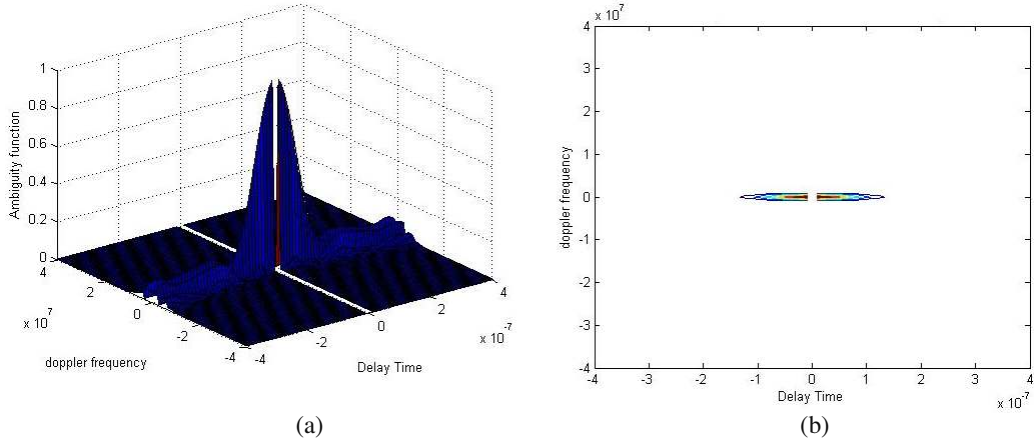
Figure 14. (a) Ambiguity functions for dual-chirp waveform as the function of Doppler frequency and time delay. (b) Contour plot.
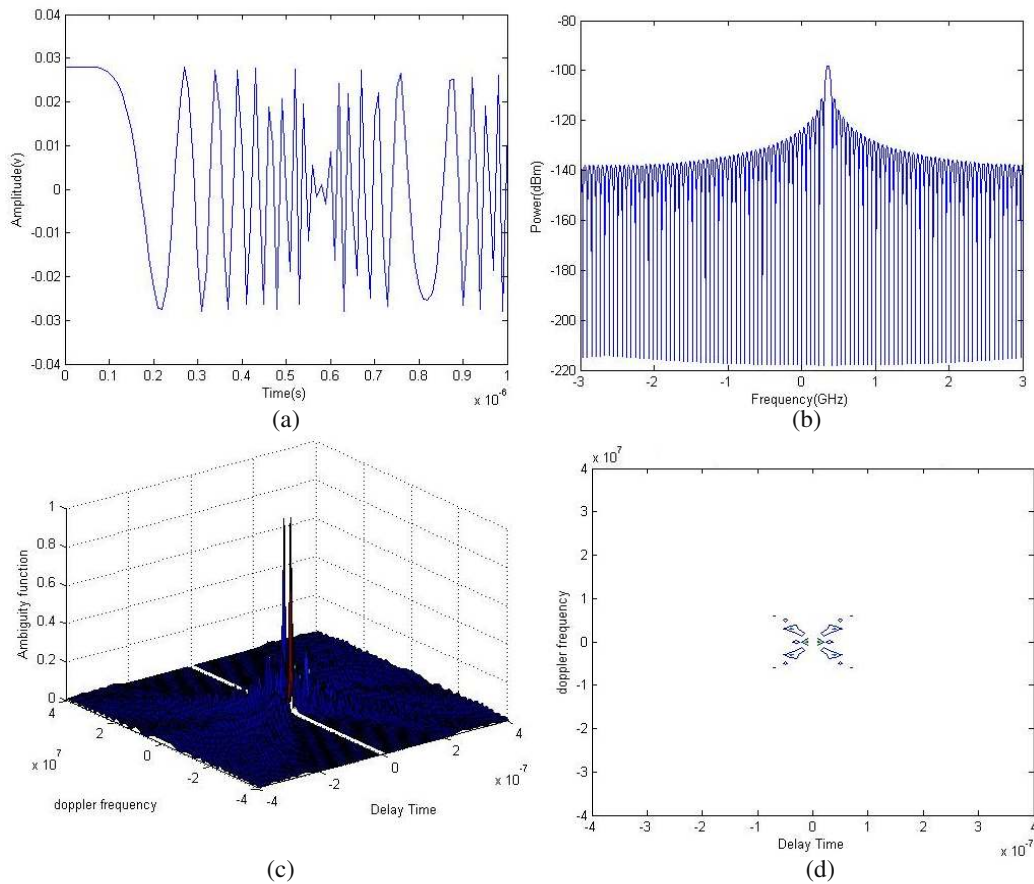
Figure 15. (a) Dual-chirp microwave waveform. (b) Power spectrum of dual-chirp signal. (c) Ambiguity functions for dual-chirp waveform as the function of Doppler frequency and time delay. (d) Contour plot.

While comparing the performance of linear chirping case versus nonlinear chirping case, it can be proved that the performance of a Radar system can be improved substantially while deploying the photonic microwave generation technique having single dual parallel mach-zehnder modulator (DPMZM) driving by nonlinearly chirped RF microwave signal.

4. CONCLUSION

In this paper, we give a complete mathematical derivation for photonics generation of dual-chirp microwave waveform using dual parallel mach-zehnder modulator (DPMZM) having linear versus nonlinear chirping capabilities. We have taken two cases of chirping, i.e., linear versus nonlinear chirp. The nonlinear chirping has a certain advantage over linear chirping in terms of increasing the chirp rate, improving the autocorrelation function and ambiguity function, as a result of an improvement of radar system. A dual-chirped microwave waveform with centre frequency 6 GHz and bandwidth 200 MHz (up to 2 GHz) is generated. The paper gives specific details about various performance parameters such as input signal frequency and power, output signal parameters viz output frequency, chirp rate, chirp bandwidth, time bandwidth product (TBW). The overall model and its performance parameters are computed through MATLAB simulation.

ACKNOWLEDGMENT

REFERENCES

1. Seeds, A. J., "Microwave photonics," *IEEE Trans. Microwave Theory Tech.*, Vol. 50, No. 3, 877–887, Mar. 2002.

2. Seeds, A. J. and K. Williams, "Microwave photonics," *J. Lightwave Technol.*, Vol. 24, No. 12, 4628–4641, Dec. 2006.

3. Capmany, J. and D. Novak, "Microwave photonics combines two worlds," *Nature Photonics*, Vol. 1, 319–330, Sep. 2007.

4. Richards, M. A., *Fundamentals of Radar Signal Processing*, 2nd Edition, McGraw-Hill, New York, NY, USA, 2014.

5. Skolnik, M. I., *Introduction to Radar Systems*, 2nd Edition, McGraw-Hill, New York, NY, USA, 2001.

6. Fitzgerald, R. J., "Effects of range-doppler coupling on chirp radar tracking accuracy," *IEEE Trans. Aerosp. Electron. Syst.*, Vol. 10, No. 4, 528–532, Jul. 1974.

7. Amar, A. and Y. Buchris, "Asynchronous transmitter position and veloc-ity estimation using a dual linear chirp," *IEEE Signal Process. Lett.*, Vol. 21, No. 9, 1078–1082, Sep. 2014.

8. Dotan, A. A. and I. Rusnak, "Method of measuring closing velocity by transmitting a dual-chirp signal," *Proc. 26th IEEE Conf. Elect. Electron. Eng. Israel*, 000258–000262, Eilat, Israel, Nov. 2010.

9. Zhu, D. and J. Yao, "Dual-chirp microwave waveform generation using a dual-parallel Mach-Zehnder modulator," *IEEE Photonics Technology Letters*, Vol. 27, No. 13, Jul. 1, 2015.

10. Iwashita, K., T. Moriya, N. Tagawa, and M. Yoshizawa, "Doppler measurement using a pair of FM-chirp signals," *Proc. IEEE Symp. Ultrason.*, 1219–1222, Honolulu, HI, USA, Oct. 2003.

11. Middleton, R. J. C., D. G. Macfarlane, and D. A. Robertson, "Range autofocus for linearly frequency-modulated continuous wave radar," *IET Radar, Sonar Navigat.*, Vol. 5, No. 3, 288–295, Mar. 2011.

12. Weigel, R., et al., "Microwave acoustic materials, devices, and applications," *IEEE Trans. Microw. Theory Techn.*, Vol. 50, No. 3, 738–749, Mar. 2002.

13. Panasik, C. M., "Multiple frequency acoustic reflector array and monolithic cover for resonators and method," U.S. Patent 6 441 703, Aug. 27, 2002.

14. Symons, P., *Digital Waveform Generation*, Cambridge University Press, New York, NY, USA, 2013.

15. Gomez-Garcia, D., C. Leuschen, F. Rodriguez-Morales, J.-B. Yan, and P. Gogineni, "Linear chirp generator based on direct digital synthesis and frequency multiplication for airborne FMCW snow probing radar," *Proc. IEEE MTT-S Int. Microw. Symp. (IMS)*, 1–4, Tampa, FL, USA, Jun. 2014.

16. Yao, J., "Photonic generation of microwave arbitrary waveforms," *Opt. Commun.*, Vol. 284, No. 15, 3723–3736, Jul. 2011.

17. Khan, M. H., et al., "Ultrabroad-bandwidth arbitrary radiofrequency waveform generation with a silicon photonic chip-based spectral shaper," *Nature Photon.*, Vol. 4, 117–122, Feb. 2010.

18. Kanno, A. and T. Kawanishi, "Broadband frequency-modulated continuous-wave signal generation by optical modulation technique," *J. Lightw. Technol.*, Vol. 32, No. 20, 3566–3572, Oct. 15, 2014.

19. Yao, T., D. Zhu, S. Liu, F. Zhang, and S. Pan, "Wavelength-division multiplexed fiber-connected sensor network for source local-ization," *IEEE Photon. Technol. Lett.*, Vol. 26, No. 18, 1874–1877, Sep. 15, 2014.

20. Li, W. and J. P. Yao, "Microwave frequency multiplication using two cascaded Mach-Zehnder modulators," *Proc. 2009 Asia-Pacific Microwave Photonics Conf.*, Beijing, China, Apr. 2009.

21. Li, W. and J. P. Yao, "Investigation of photonically assisted microwave frequency multiplication based on external modulation," *IEEE Trans. Microw. Theory Tech.*, Vol. 58, No. 11, 3259–3268, Nov. 2010.